Driver Activity Monitoring Based On Modulated Frequency Selective Surface and Millimeter-Wave Radar

F. Morabet, A. Lazaro, *Senior, IEEE*, M. Lazaro, R. Villarino, and D. Girbau *Senior, IEEE*

***Abstract*— In-cabin wireless sensors are vital for enhancing road safety and enabling autonomous vehicle technologies. Current vehicles use internal sensors to detect seat belt status, occupant presence, and driver behaviors. Early detection of inattentiveness or erratic driving can significantly reduce accident risks. In this context, this work presents a novel driver activity monitoring system based on a modulated Frequency Selective Surface (FSS), which is read by means of a millimeter-wave Doppler radar for detecting driver head movements. The proposed system offers a non-invasive, privacy-preserving approach by modulating the FSS at two distinct frequencies, enabling precise detection of key head gestures. By focusing on only two modulated frequencies instead of monitoring the entire head and its surrounding area, the system significantly reduces computational complexity and enhances noise immunity, which is essential for in-vehicle applications, where vibrations play an important role. This reduction also simplifies hardware requirements and enables faster, real-time processing, making it highly suitable for integration into Advanced Driver Assistance Systems (ADAS) and vehicle safety monitoring applications. The system aims to distinguish between the driver's attention and non-attention states. Experimental evaluations demonstrate the system's effectiveness in achieving this goal while providing lower hardware complexity compared to traditional approaches. By continuously monitoring driver head movements, the proposed system facilitates timely, proactive interventions to mitigate risks and enhance overall road safety.**

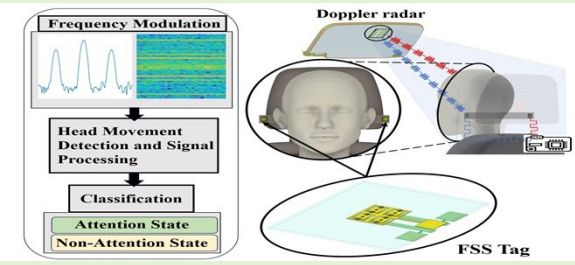

***Index Terms*— In-cabin sensors, Frequency Selective Surface (FSS), Millimeter-Wave radar, driver head movement detection, non-invasive monitoring, Advanced Driver Assistance Systems (ADAS), real-time processing, driver attention detection.**

I. Introduction

THE integration of in-cabin vehicle sensor technology is increasingly vital for road safety, making it essential for both conventional and future smart vehicles. Among its applications, monitoring the driver's mental health and psychological well-being has gained attention due to its potential to reduce one of the leading causes of traffic accidents. Stress, anxiety, and other mental health issues can significantly impair driving performance and raise accident risk [?], [?]. Additionally, the World Health Organization's 2023 Global Status Report on Road Safety states that road traffic crashes claim approximately 1.19 million lives each year, particularly affecting younger populations [?]. This alarming statistic highlights road traffic accidents as a major global cause of death. Moreover, a comprehensive study conducted by the National Highway Traffic Safety Administration (NHTSA) emphasizes the severe risks that driver distractions pose to road safety. The report highlights that cognitive distractions, such as using mobile devices, eating, or interacting with passengers, significantly elevate the likelihood of a crash. Alarmingly, in 2021, distracted driving was implicated in 8.5% of all fatal crashes, leading to the tragic loss of over 3,000 lives. This study underscores the importance of addressing these distractions to enhance safety and reduce the prevalence of fatal accidents on the roads [?].

In light of these challenges, advanced driver monitoring systems have been developed to detect various safety-related indicators and risk factors [?]. These systems use diverse methodologies, such as monitoring vehicle operations [?], [?] and directly assessing physiological parameters through detection systems, including distributed cameras [?], [?], wearable devices [?], [?], and various sensors [?], [?]. Among these, radar sensors have proven especially effective for non-contact detection, offering consistent performance in varying lighting, improving privacy and security, environmental resilience, and reduced processing needs, all while avoiding wear and tear [?].

Manuscript received August 22, 2023; accepted January xx, 2023. Date of publication January xx, 2023; date of current version August 22, 2023. This research was funded by the projects PID2021-122399OB-I00 MICIU/AEI/10.13039/501100011033/FEDER, UE, and TED2021-130307B-I00 MICIU/AEI/10.13039/501100011033/ European Union NextGenerationEU/PRTR, and the grants PRE2019-089028.

The authors are with the Electronics, Electrical and Automatics Engineering Department, Rovira and Virgili University, Tarragona, Spain (e-mail: farid.morabet@urv.cat, antonioramon.lazaro@urv.cat, marc.lazaro@urv.cat, ramon.villarino@urv.cat, david.girbau@urv.cat). The corresponding author is A. Lazaro (e-mail: antonioramon.lazaro@urv.cat).

Moreover, radar-based systems provide a non-intrusive, reliable solution for driver monitoring, performing robustly across diverse conditions without requiring driver interaction [?], [?]. This non-intrusive approach enhances both system effectiveness and user comfort. Combining multiple data sources allows these systems to provide comprehensive detection capabilities essential for heightened situational awareness and preventive measures. This can help reduce risks linked to psychological distress, cognitive distractions, and medical impairments while driving [?].

Radar-based monitoring systems use advanced non-contact technologies to monitor driver behavior and physiological signals. These technologies are known for their ability to detect micro-movements, such as respiration, with high sensitivity and resolution [?]. Other systems are particularly effective in tracking larger body movements by leveraging the Doppler effect to measure motion and velocity [?]. Some radar systems further integrate range and velocity measurements, allowing precise tracking of the driver's position and movements [?], making them highly suitable for comprehensive monitoring applications. Recently, several works about seat occupancy based on mm-wave radars have been proposed [?], [?], [?], [?].

While traditional radar technologies have proven effective in driver monitoring, they face limitations highlighting the need for a novel approach [?]. Some radar technologies excel at detecting micro-movements, such as respiration or heart rate [?], but struggle with tracking specific movements, like head gestures, reducing their applicability in comprehensive monitoring scenarios [?]. Other systems, though adept at measuring motion and velocity, often lack the precision needed to differentiate between various types of movements, leading to potentially ambiguous interpretations of driver behavior [?]. Combined systems that offer both range and velocity measurements tend to introduce complexity and higher costs due to advanced signal processing and multiple antennas [?].

Addressing these challenges, this paper proposes a novel driver monitoring system that leverages the simplicity and efficiency of modulated FSS, which is read with an mmWave radar system to track head movements specifically. By utilizing two modulated FSS with a square waveform at distinct frequencies, the proposed approach ensures easier implementation and is more robust to clutter interference. The use of a simple Doppler radar significantly reduces the computational burden, making the system more suitable for real-time processing with lower hardware requirements. This method not only offers a robust and privacy-preserving solution for monitoring driver behavior but also reduces hardware requirements, making it more suitable for real-time implementation in modern driver assistance systems.

Thus, this work aims to fulfill three key objectives: 1) developing a robust, privacy-preserving driver monitoring system that accurately detects head movements by optimizing the modulation of FSS read by an mmWave radar; 2) implementing a reliable real-time monitoring solution to distinguish between attention and non-attention states, leveraging head movement data and radar signal processing, and 3) conducting experiments to validate the accuracy and reliability of the proposed system in diverse real-world driving conditions, ensuring its practical feasibility for ADAS.

This article is organized as follows: Section II provides a detailed overview of the head movement patterns relevant to driver behavior and their implications for road safety. Section III details the methodology and system components, including experimental design and signal processing techniques. Section IV and Section V present the experimental setup and results, respectively, showcasing the system's performance. Finally, Section VI concludes the paper and suggests directions for future research.

II. Driver Head Movement in Automotive Context

This section introduces the fundamental concepts of driver behavior, focusing on how head movements can reveal a driver's cognitive and physiological state. Key movement patterns such as yaw, pitch and roll offer insights into the driver's awareness, focus, and stress levels. In typical driving conditions, these movements are constrained by the vehicle's interior layout and the driver's need to maintain control, resulting in specific, defined ranges for head motion, as shown in Fig. 1. Studies included in [?], show that driving head movements include a yaw range of about 88°, enabling drivers to check mirrors and blind spots. Pitch movements generally fall within 45°, allowing drivers to glance between the dashboard, speedometer, and forward view. Roll movements are often limited to about 20°, support controlled tilts that enhance visibility and control. Together, these movements ensure the driver's attention to the road and in-car elements. Analyzing these specific head movement patterns enables the development of advanced Driver Monitoring Systems (DMS) and fatigue detection technologies. Such systems help reduce accidents due to inattention, distraction, or aggressive driving. This section assesses the head movement indicators related to different states of driver attention, distraction, and aggressive behavior, providing a foundation for further advancements in road safety technology.

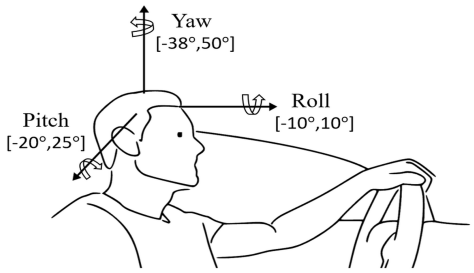

Fig. 1. Defined Ranges for Driver Head Movements: Yaw, Pitch, and Roll Angles.

Understanding the significance of head movements in assessing driver behavior is critical for the development of advanced DMS and road safety technologies. To ensure an accurate analysis of the driver's state, specific head movements have been categorized based on their correlation with different driving conditions. These movements, as summarized

TABLE I
HEAD MOVEMENTS ASSOCIATED WITH DRIVER STATES

State	Key Head Movements	Description	Reference
Attention	Frequent Yaw Movements (Horizontal)	Indicates active engagement with driving tasks, such as checking mirrors and scanning for hazards.	[?]
	Head Roll Movements (Side-to-Side Tilt)	Unintentional side-to-side tilt, often linked to fatigue and used as a predictor in driver monitoring systems.	[?]
	Prolonged Forward Pitch Movements	Associated with microsleep episodes, leading to a temporary loss of situational awareness.	[?]
Distraction	Extended Lateral Yaw Movements	Prolonged sideways movements indicate distraction, such as engaging with passengers or in-car objects.	[?]
	Erratic Yaw and Pitch Movements	Sudden, irregular movements caused by secondary tasks (e.g., mobile phone use), indicating attention shifts.	[?]
Aggression	Rapid Yaw Movements	Quick, sharp movements are often observed when preparing for abrupt maneuvers, such as aggressive lane changes or speeding.	[?]
	Tense Pitch Movements	Rapid, tense movements during acceleration or braking, indicating impatience and aggressive behavior.	[?]

comprehensively in Table I, provide key insights into the physiological and cognitive states of drivers, allowing systems to distinguish between attention and non-attention states.

The following section describes the proposed system for detecting the driver's head movements using a Doppler radar as a sensor, as well as the modulation of the FSS and its design at 24 GHz.

III. METHODS AND TECHNOLOGIES

A. Method Overview

The system for monitoring driver head movements proposed in this paper is based on two fundamental components: two modulated FSS tags and radar. The two modulated FSS tags are mounted on the left and right sides of the headrest, each operating at distinct frequencies f_{m1} and f_{m2}. These frequencies allow the system to differentiate between the signals reflected from each side, enabling the determination of the driver's head position through differential backscattered signals. The second element is a 24 GHz radar, which is mounted on the sun visor. This reader, equipped with high-gain directional transmission and reception antennas and a low-noise receiver, sends the signal and captures and processes the modulated signals that are backscattered at the FSS tags. The system's operation is illustrated in the block diagram shown in Fig. 2. The relative position of the FSS tags with respect to the head. Depending on the head position or movement, the visibility of the tags by the radar changes.

1) Signal Modulation: The FSS tags modulate their radar cross-section (RCS) through the controlled switching of PIN diodes. These diodes alter the reflection characteristics of the FSS, thereby influencing how incoming electromagnetic waves are backscattered toward the radar. The radar system initially emits a continuous wave (CW) signal. When this incident signal E_{incident} strikes the FSS, it induces currents on the surface of the FSS elements. The PIN diodes, integrated within the FSS, modulate these induced currents by switching between active (ON) and inactive (OFF) states [?]. This

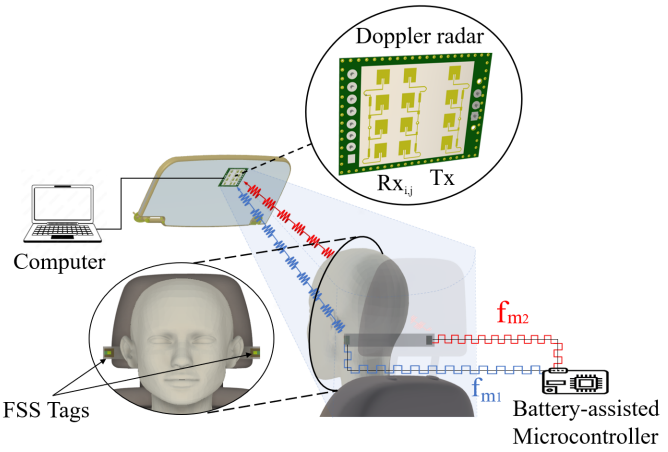

Fig. 2. System overview illustrating FSS-based signal modulation and Doppler radar detection of driver head movements.

modulation alters the reflection coefficient of the FSS and results in a modulated scattered field.

The backscattered field at the FSS $E_S(f)$ can be split into the sum of two terms: a non-modulated structural mode ($E_{structural}$) and a modulated tag mode [?], [?]:

$$E_S(f) = E_{structural}(f) + \Gamma(f) E_{\text{incident}} \tag{1}$$

Assuming that the switching frequency ($f_m = 1/T_m$) is much lower than the carrier frequency of the incoming wave, the reflection coefficient at the carrier frequency varies over time following a square waveform [?]:

$$\Gamma(t) \approx \Gamma_{OFF} + (\Gamma_{ON} - \Gamma_{OFF}) \sum_{n=0}^{n=\infty} rect\left(\frac{t - nT_m}{T_m}\right) \tag{2}$$

where Γ_{ON} and Γ_{OFF} are the reflection coefficients at the carrier frequency (f_c) for the ON and OFF PIN diodes states, respectively, and the function $rect()$ denotes the unity rectangular pulse. As the reflection coefficient (2) is a periodic

function, it can be expanded using a Fourier series:

$$\Gamma(t) = \sum_{k=-\infty}^{k=+\infty} c_k e^{j2\pi k f_m t} \tag{3}$$

Then, the reflection coefficient in the frequency domain is a sum of delta functions:

$$\Gamma(f) = \sum_{k=-\infty}^{k=+\infty} c_k \delta(f - (f_c + k f_m)) \tag{4}$$

where the Fourier coefficients c_k are:

$$c_k = \begin{cases} \frac{(\Gamma_{ON}+\Gamma_{OFF})}{2} & , k = 0 \\ \frac{(\Gamma_{ON}-\Gamma_{OFF})}{2} \frac{sin(k\pi/2)}{k\pi/2} & , k \neq 0 \end{cases} \tag{5}$$

From this analysis, the term $k = 0$ corresponds to the backscattered field at f_c, which is the sum of the structural field and the average reflected field in the FSS. Due to modulation, infinite sidebands appear, spaced at integer multiples of the modulation frequency $f = f_c + k f_m$. Their amplitudes are proportional to the Fourier coefficients, which rapidly decay with increasing k. Practically, only the first sidebands at frequencies ($f_c \pm f_m$) are detected, as higher harmonics generally fall below the receiver's noise floor and cannot be detected.

As in RFID systems, the detected power at the first sidebands is proportional to the differential radar cross-section, which measures the difference in backscattered power between the ON and OFF states at the first sidebands. This differential radar cross-section can be expressed as [?], [?]:

$$\Delta\sigma_d = 4\pi r^2 \left(\frac{|E_{\text{ON}} - E_{\text{OFF}}|}{|E_{\text{incident}}|} \right)^2 \tag{6}$$

Where E_{ON} and E_{OFF} Represent the backscattered electric field amplitude when the PIN diodes on the FSS are in the ON and OFF states, respectively. This differential RCS can be expressed as a function of the RCS of a plate σ_{plate} multiplied by the differential reflection coefficient $\Delta\Gamma = \Gamma_{ON} - \Gamma_{OFF}$, and a modulation factor given by $m = |c_1/\Delta\Gamma|^2$:

$$\Delta\sigma_d = \sigma_{plate} \left|\Delta\Gamma\right|^2 m \tag{7}$$

This differential scattering effect due to the modulation induced by the PIN diodes is what enables the radar system to detect and analyze the modulated signals, allowing for effective monitoring of driver head movements. Notably, clutter reflections (e.g. reflections from other objects in the vehicle) are not modulated and contribute to the signal at the carrier frequency only [?], [?]. Therefore, these reflections can be separated on the radar.

2) RADAR Detection: After the FSS tags modulate the radar cross-section (RCS) through the switching of PIN diodes, the radar system processes the backscattered signals to isolate the modulated frequencies and determine the driver's head position. The received signal at the radar is down-converted using an in-phase/quadrature (IQ) mixer. The IQ outputs are sampled using the analog-to-digital converter (ADC) included in the microcontroller embedded in the radar at a sampling rate of 9 kHz. Then, the baseband spectrum is obtained by applying a Fast Fourier Transform (FFT) to convert the sampled complex time-domain signal $x[n] = i[n] + jq[n]$ into the frequency domain. A Hamming Window is applied before computing the spectrum to reduce the effects of the finite length of samples (windowing), and zero padding is used to improve the frequency resolution.

The resulting spectrum $X(f)$ displays peaks at the modulation frequencies introduced by the PIN diodes, corresponding to the specific modulation patterns of the FSS tags. The presence of these peaks indicates the presence of the modulated signals, which are key to determining the driver's head position. Static reflections associated with objects fall close to the direct current (DC) baseband spectrum. Even reflections caused by small passenger movements, which introduce small frequency shifts due to the Doppler effect, contribute far from the selected modulated frequencies [?]. This characteristic is highly advantageous for detecting head movements, as changes in received power at the modulating frequencies occur only when the head partially obstructs the FSS's line of sight.

To determine the relative position of the driver's head, the radar system calculates the Differential Power Variation (DPV) ΔP_r, between the two modulated frequencies. This measure reflects the relative strength of the signals modulated by the FSS tags, enabling precise head movement detection. The calculation is given by:

$$\Delta P_r = P_r(f_{m1}) - P_r(f_{m2}) \tag{8}$$

Where $P_r(f_{m1})$ and $P_r(f_{m2})$ are the received power at the modulation frequency corresponding to the first tag Tag 1 (f_{m1}) and Tag 2 (f_{m2}), respectively.

A positive ΔP_r indicates the driver's head is closer to Tag 1, while a negative value suggests proximity to Tag 2. By continuously monitoring these changes, the radar system can track head movements in real-time, enabling integration with vehicle safety systems for alerts or corrective actions if abnormal movements are detected.

B. FSS Design

The proposed antenna builds upon the foundation of a standard electronically switchable FSS [?], known for its stable frequency response while using a microcontroller-based modulation method established in prior research [?]. This work introduces a significant modification: repurposing the FSS as a backscatter element specifically designed to interface with a Continuous Wave (CW) Doppler radar operating at a resonance frequency of 24 GHz. This adaptation enhances the differential radar cross-section while ensuring low power consumption, which is critical for practical high-frequency applications.

The dimensions of the unit cells in Frequency Selective Surfaces (FSS) are crucial as they determine the frequency-selective properties of the surface. The maximum dimensions of the FSS unit cell are related to the wavelength of the operating frequency. Grating lobes are unwanted diffraction effects that occur when the periodicity of the FSS elements is comparable to or greater than the wavelength of the incident

wave. These lobes can cause interference and degrade the performance of the FSS. To minimize grating lobes, the spacing between the elements should be less than half the wavelength of the highest frequency of interest [**?**]. Miniaturization contributes to improved performance and stability for different angles of incidence and polarization [**?**]. In this work, a unit cell close to a quarter wavelength in free space at 24 GHz (12.5 mm) has been selected, which is compatible with the diameter of the via hole. The dimensions of the square loop and inner patch are adjusted to obtain the desired resonance frequency at 24 GHz, taking into account the parasitics introduced by the PIN diodes.

The FSS units are fabricated using a 17 µm copper layer on a Rogers 4003 dielectric substrate [**?**], selected for its high performance at high frequencies. The substrate has a relative permittivity of 3.45, a loss tangent of 0.0031, and a thickness of 0.51 mm. The unit cell geometry, illustrated in Fig. 3(a), consists of a square loop aperture, a connecting pin, and a base layer, with final dimensions of 3 mm × 3 mm. The inner square loop measures 1.7 mm, with a uniform gap of 0.35 mm between the inner and outer squares and an additional 0.3 mm gap on each side to ensure consistent performance.

For switching under oblique incidence, two MADP-000907-14020x Aluminum Gallium Arsenide (AlGaAs) flip-chip PIN diodes [**?**] are placed on opposite sides of the aperture. The diodes, with low series resistance R_{ON} = 5.2 Ω, R_{OFF} = 7.2 MΩ and low capacitance (C_{OFF} = 0.025 pF), provide efficient operation and minimal signal loss in both ON and OFF states. Their rapid switching speed (2 ns) makes them ideal for this application. The configuration, with a centrally located thru-pin for negative DC biasing and positive biasing at the aperture's corners, ensures effective impedance control and robust switching performance.

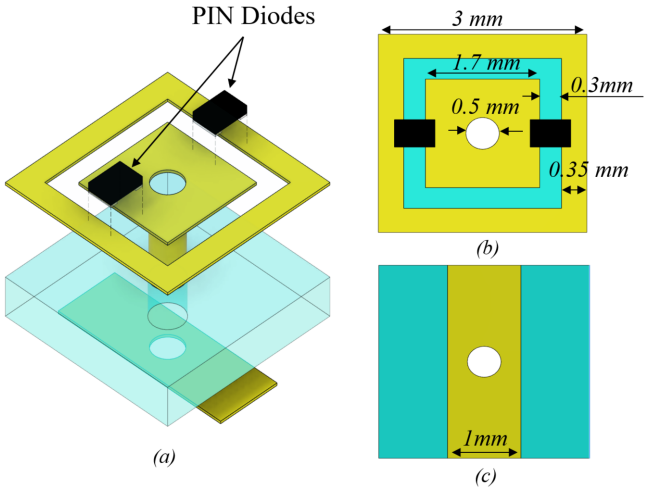

Fig. 3. Structural Design and Dimensions of the FSS Unit Cell. a) Exploded view illustrating the multi-layered structure of the FSS. b) Top view. c) Side view.

To facilitate understanding and prediction of the electromagnetic (EM) behavior of the FSS frequency response at 24 GHz, an equivalent circuit model (ECM) was developed using a lumped element approach [**?**], [**?**]. The proposed unit

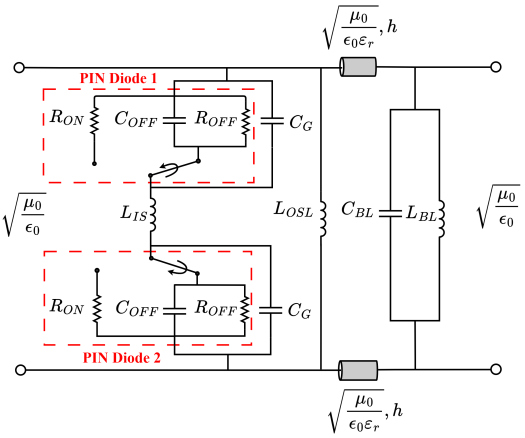

Fig. 4. Equivalent Circuit Model of the FSS Unit Cell for the two diode states (ON/OFF).

cell can be modeled by the equivalent circuit shown in Fig. 4. where each inductive, resistive, and capacitive element is designed to reflect the physical and electromagnetic properties of the FSS structure, with $\sqrt{\mu_0/\epsilon_0}$ representing the wave impedance of free space. The outer square loop inductance, L_{OSL}, governs the low-frequency response, while the inner square loop inductance, L_{IS}, fine-tunes the high-frequency resonance. The bias line inductance, L_{BL}, ensures impedance matching and stable performance. Additionally, a coupling capacitance, C_{BL}, between the bias line and resonator captures the mutual electromagnetic interaction, enhancing frequency selectivity and preventing interference. To further refine the frequency response, a gap capacitance, C_G, is included to model the small gaps between conductive elements within the unit cell, allowing for precise control of EM coupling and maintaining the desired resonant frequency. The PIN diodes themselves have distinct ON and OFF state resistances, where a low ON-state resistance minimizes signal loss, and a high OFF-state resistance ensures high isolation, preventing signal leakage and maintaining robustness. The capacitance in the OFF state complements this isolation by mitigating any residual leakage effects, which is critical for maintaining high isolation and a sharp resonant behavior. Table II summarizes the values of the lumped elements of the FSS in free space at 24 GHz.

Before finalizing the FSS geometry, a detailed comparison of the unit cell's scattering parameters was conducted using both ANSYS HFSS and ADS simulations, as shown in Fig. 5. The full-wave simulations in HFSS and the circuit-based ADS models exhibit a strong correlation, confirming the accuracy of the proposed ECM in predicting the resonance characteristics at 24 GHz. Although minor discrepancies between the two methods are present, primarily due to HFSS's ability to capture more detailed electromagnetic interactions, the simulations consistently highlight the significant differences between the ON and OFF states of the FSS unit cell, emphasizing its modulation capabilities. In the OFF state, a deeper S_{11} resonance dip is observed, reaching below -15 dB at 24 GHz. This signifies effective impedance matching and minimal reflection due to stronger electromagnetic coupling from the high OFF-state

TABLE II
VALUES OF THE PARAMETERS OF THE LUMPED-MODEL FSS

C_{BL}	C_G	L_{OSL}	L_{IS}	L_{BL}
0.016 pF	0.072 pF	0.85 nH	0.124 nH	1.94 nH

resistance and low capacitance of the PIN diodes. In contrast, when the diodes are in the ON state, their low ON-resistance causes the incident signal to be largely reflected, experiencing minimal losses of approximately 0.5 dB. These distinct S_{11} profiles validate the FSS's capability to effectively modulate reflected signals from 24 GHz radar systems.

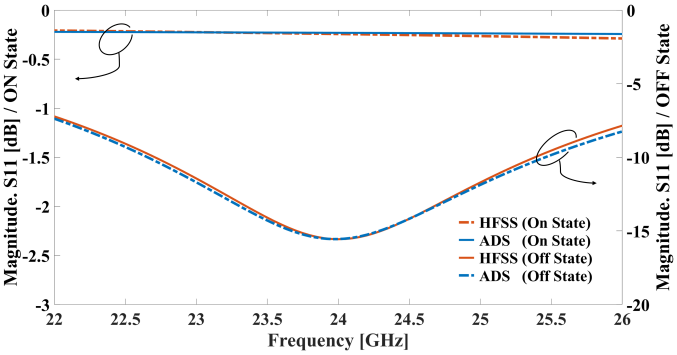

Fig. 5. Simulated Reflection Coefficient S11 of the FSS Unit Cell in ON and OFF States.

Reliable modulation of the reflected radar signal is achieved through the proposed FSS prototype, incorporating a 2 × 2 array of unit cells, as illustrated in Fig. 6, with additional components integrated into the design. Soldering pads are placed on the top side for the positive DC bias and on the rear side for the negative DC bias, allowing connection to an external frequency generator for biasing the PIN diodes. To prevent interference with RF operation and avoid unwanted load effects from the bias lines, two 1 kΩ resistors are incorporated into the negative DC bias lines to isolate the RF signal from the biasing network. A comprehensive experimental setup was established to investigate the modulation characteristics of the FSS, as depicted in Fig. 7. The configuration includes a signal generator DS Instruments SG30000, which transmits a continuous wave (CW) signal at 24 GHz, at a power level of 10 dBm, which is transmitted via a wideband horn antenna (T_X) with a 20 dB gain, placed 60 cm away from the FSS. Modulation is performed using a square waveform produced by a low-frequency signal generator (Agilent 33521A), which toggles the PIN diodes between their active ON state (0V) and OFF state (-3V). The modulated backscatter was subsequently captured by a receiving horn antenna (R_X) with identical specifications. The received signal is then analyzed using a Rohde & Schwarz FSP spectrum analyzer, connected to a computer for data acquisition and processing.

Fig. 8 shows the measured spectrum, with a strong central peak at 24 GHz (-47 dBm), indicating direct coupling between the transmitter and receiver, and with clear sideband peaks (-58 dBm)at the modulation frequency. The spacing of the sidebands (± 1 kHz) further confirms successful modulation at the applied frequency. Fig. 9 shows the received power

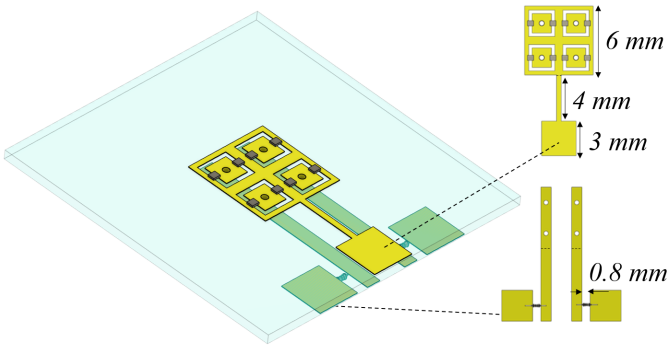

Fig. 6. Isometric view of the Proposed FSS tag.

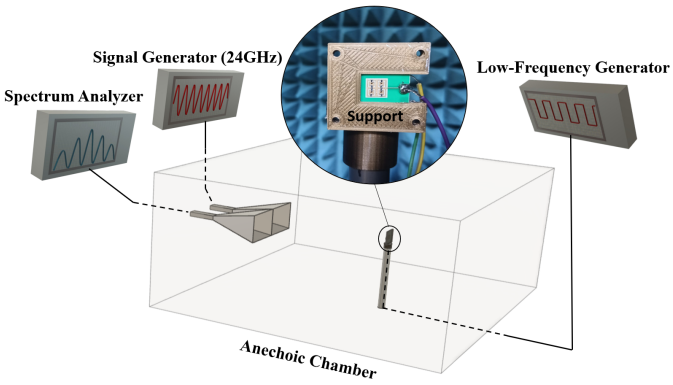

Fig. 7. Schematic setup for evaluating the FSS modulation performance.

spectrum of the first sideband in the signal modulated at the FSS tag as a function of the carrier frequency, spanning a 4 GHz bandwidth.

In this work, a continuous wave (CW) radar transmitting at a single frequency of 24 GHz is used. However, the bandwidth achieved allows the use of other types of radar, such as frequency-modulated continuous wave (FMCW) radars, which have a wider bandwidth. Another advantage of the wide bandwidth of the FSS is its robustness to response drifts caused by manufacturing tolerances. The modulation frequency is only limited by the switching time of the PIN diodes, which is 2 ns according to the manufacturer's datasheet. Therefore, it is possible to modulate at frequencies of up to several MHz. However, in this work, the limitation of the modulation frequency is given by the bandwidth of the ADC. To measure velocity with the Doppler radar, the internal ADC of the board itself is used, selecting a sampling frequency of 9 kHz. Thus, according to the Nyquist sampling theorem, the modulation frequency is limited to 4.5 kHz, which can be easily generated by the microcontroller using one of the digital outputs.

IV. EXPERIMENT SETUP AND DATA COLLECTION

The experiments were conducted to evaluate the proposed driver activity monitoring system under real situations to ensure consistent and reliable performance of the system for vehicular applications, since this is a very unfavorable application mainly due to vibration during mobility. The test vehicle was equipped with a low-cost 24 GHz Doppler radar

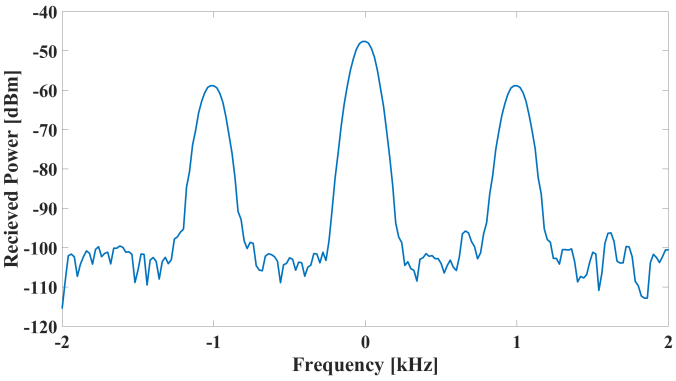

Fig. 8. Power Spectrum of FSS Tag-Modulated Signal at 24 GHz with ±1 kHz Sideband Modulation

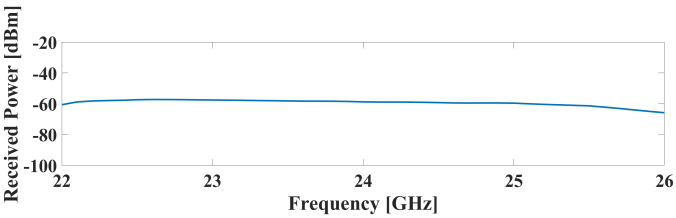

Fig. 9. Received Power Spectrum of FSS Tag-Modulated Signal at the first side-band as a function of the carrier frequency.

sensor (RFbeam K-LD7) [?], [?], mounted on the sun visor and configured to detect and track driver head movements. Two FSS tags were integrated into the driver's headrest, each modulated at distinct frequencies of 1 kHz and 0.7 kHz for Tag 1 and 2, respectively. In the prototype, an Atmel ARM Cortex-M0 ATSAM21G18A-MU microcontroller with a clock frequency of 48 MHz was used to generate the modulating signals using the Pulse Width Modulation (PWM) output of a microcontroller. The typical output power of the radar is 6 dBm. The radar uses a 3x4 patch antenna array with 8.6 dBi gain and an 80° horizontal beamwidth and a 34° vertical beamwidth, focusing detection on the headrest area to accurately capture even subtle head movements. The radar has signal processing capabilities, performing 256-point FFT for initial analysis in the frequency domain. However, to achieve higher resolution and reduce the noise floor, the experiments utilized external processing. Raw IQ samples from the radar's ADC were transmitted via a microcontroller to a host computer for advanced analysis. On the host, MATLAB performed a 2048-point FFT on the raw data, replacing the radar's internal FFT. This external processing allowed the system to resolve closely spaced frequencies more accurately, enhancing detection and tracking capabilities. By leveraging the larger FFT, the system effectively distinguished fine movements in the challenging vehicular environment.

Head movements were quantified using the DPV, as defined in Section III-A, representing the difference in received power between modulated frequencies associated with Tag 1 and Tag 2. To enhance signal quality, wavelet denoising was applied to both signals, reducing high-frequency noise while preserving low-frequency components indicative of driver head movements. A dual-threshold approach was employed to identify significant movement points. Specifically, significant movements occur when notable changes are observed in both signals, even if one shows more change than the other. This approach helps to prevent false positives that may arise from significant changes in only one signal. Consequently, a point was classified as a significant movement if it met either of the following conditions:

Condition 1:

$$|P_{s1,d}[i]| > \tau_{s1}^{\text{high}} \quad \vee \quad |P_{s2,d}[j]| > \tau_{s2}^{\text{low}} \tag{9}$$

Condition 2:

$$|P_{s1,d}[i]| > \tau_{s1}^{\text{low}} \quad \vee \quad |P_{s2,d}[j]| > \tau_{s2}^{\text{high}} \tag{10}$$

Where:

- $P_{s1,d}[i]$ and $P_{s2,d}[j]$ represent the denoised power changes in the signal of both tags at points i and j, respectively.
- τ_{s1}^{high}, τ_{s2}^{high}: High threshold for signal associated with Tag 1 and Tag 2, respectively.
- τ_{s1}^{low}, τ_{s2}^{low}: Low threshold for signal associated with Tag 1 and Tag 2, respectively.

Both conditions require that these power changes occur within a time tolerance Δt_{tol}, ensuring that the two points t_i and t_j are temporally correlated:

$$|t_i - t_j| \leq \Delta t_{\text{tol}} \tag{11}$$

Points that met either condition were marked as significant movements. These individual movement points were then grouped into significant movement regions based on a proximity threshold, $\Delta t_{\text{cluster}}$. To form clusters, the first significant movement point served as the starting reference, and each subsequent point t_k was added to the cluster if it satisfied the proximity condition:

$$|t_k - t_{k-1}| \leq \Delta t_{\text{cluster}} \tag{12}$$

This process is visually depicted in Fig. 10, which illustrates a single scenario (Condition 1). The figure breaks down each step and visually explains how the thresholds (τ_{s1}^{high} and τ_{s2}^{low}) were applied to identify significant movement points. It further shows how temporal correlation (Δt_{tol}) ensures valid pairings between the signals, and how proximity constraints ($\Delta t_{\text{cluster}}$) are used to group these points into clusters of significant movements.

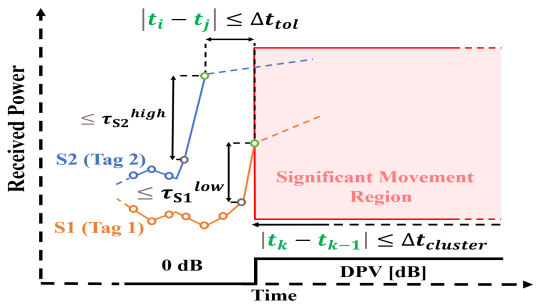

Fig. 10. Visualization of Dual-Threshold and Temporal Constraints for a Single Scenario: Condition 1

The calibration process, as summarized in Table III, involved testing with several volunteers under real-world conditions. Each volunteer adjusted the driver's seat and simulated driving scenarios, introducing variability in the radar-to-seat distance and individual dimensions (height and weight). This testing captured the average DPV, along with maximum differences in DPV values for non-significant and significant movements. These results provided critical insights into setting detection thresholds. The specific parameter values in Table IV were determined based on these calibration results. The thresholds τ_{high}^{s1} and τ_{high}^{s2} were derived as one-quarter of the mean value of the measured DPV, ensuring sensitivity to significant head movements while avoiding false positives caused by minor variations or noise. Furthermore, τ_{low}^{s1} and τ_{low}^{s2} were set to 2 dB, based on the standard deviation introduced by car vibrations. Calibration results in Table III confirmed that non-significant movements did not simultaneously reach or exceed 4 dB and 2 dB for $P_{s1,d}[i]$ and $P_{s2,d}[j]$, as required by the dual-threshold conditions defined in Eq. (9) and Eq. (10). In contrast, significant movements consistently satisfied these conditions, highlighting the robustness of the thresholds. The parameter $\Delta t_{\text{cluster}}$ was chosen to represent the typical duration for which a driver moves their head to check mirrors, while Δt_{tol} was set to the interval between consecutive samples, ensuring accurate detection and analysis of significant head movements. In Section V, these thresholds were validated with real-world testing, confirming their reliability across diverse scenarios.

TABLE III
MEASUREMENTS OF DPV AS A FUNCTION OF THE VOLUNTEER

Gender	Height (m)	Weight (kg)	Distance to Radar (cm)	avg. Mean DPV	Max Diff. $[P_{s1,d}[I], P_{s2,d}[j]]$ (Non-Significant	Max Diff. $[P_{s1,d}[I], P_{s2,d}[j]]$ (Significant)
Male	1.81	76	60	15.1	[3.6, 3.3]	[15.8, 11.0]
Male	1.66	64	60	13.9	[4.7, 1.3]	[12.8, 11.7]
Female	1.69	67	60	14.7	[3.4. 3.2]	[14.6, 10.2]
Female	1.75	72	65	15.4	[3.1, 2.0]	[14.2, 6.8]
Male	1.82	83	75	15.8	[2.8, 1.7]	[11.5, 4.1]

TABLE IV
PARAMETER SPECIFICATIONS FOR REAL-TIME MOVEMENT TRACKING

τ_{s1}^{high}	τ_{s1}^{low}	τ_{s2}^{high}	τ_{s2}^{low}	Δt_{tol}	$\Delta t_{\text{cluster}}$
4 dB	2 dB	4 dB	2 dB	100 ms	2 s

The experiments were designed to simulate typical driving scenarios under conditions replicating real-world environments. Fig. 11 illustrates the experimental setup used for all measurement tests, including the radar sensor mounted on the sun visor and the FSS tags positioned on the headrest. Each test was conducted with identical setup conditions over the same period to ensure stable radar system performance and reliable comparisons.

V. RESULTS AND ANALYSIS

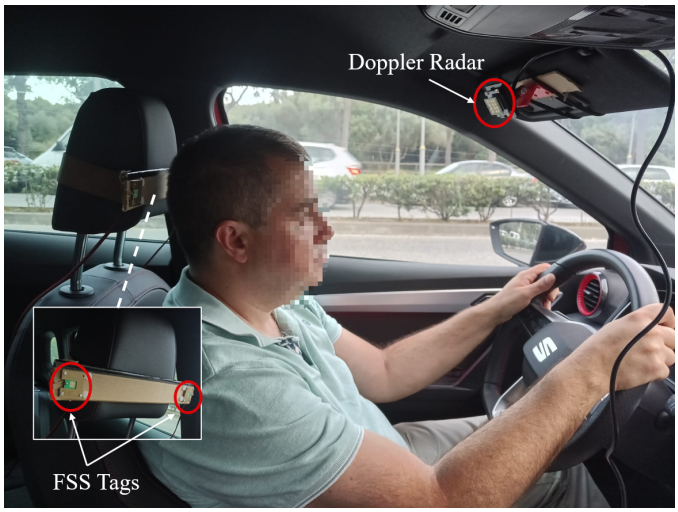

Fig. 11. In-Vehicle Experimental Setup

Initial experiments were conducted with the vehicle stationary, focusing on the system's capability to detect and distinguish between driver attention and non-attention states without the influence of external driving variables. First, to validate the effectiveness of the proposed system, an experimental evaluation was conducted to simulate typical driving scenarios as outlined in Section II. The filtered DPV signal, as shown in Fig. 12, illustrates the variations in received power between Tag 1 (modulated at 1 kHz) and Tag 2 (modulated at 0.7 kHz) over a one-minute period. Regions where head movements exceed the set threshold are highlighted and labeled as Regions "1" through "6", with a summary of observed behaviors and their implications provided in Table V for clarity.

The bar chart in Fig. 13 illustrates how the system detects significant movement regions, as highlighted in Fig. 12, by showing the maximum values of $P_{s1,d}[i]$ and $P_{s2,d}[j]$ for each region. The thresholds for significant movements, as defined in Table IV, are consistently met in these regions, while minor variations or noise remain below the specified values. This highlights the system's ability to reliably distinguish meaningful head movements from irrelevant fluctuations.

Furthermore, the time-frequency spectrogram illustrated in Fig. 14 provides additional validation of the observed head movements depicted by the DPV signal, presenting the time-frequency distribution of the received radar signals, and demonstrates the system's ability to detect the presence of modulated frequencies and their harmonics. The clear separation between the modulation frequencies of Tag 1 and Tag 2 confirms the system's capability to identify signal variations corresponding to different driver head positions that are critical for monitoring driver behavior in real-time under several realistic driving scenarios, such as the ones explained in the next paragraphs. As observed in the spectrogram in Fig. 14, the movements of the driver's body or the actions of the passengers cause an increase in the spectrum level around the Doppler frequency associated with the radial velocity of such movements. These interferences appear near zero frequency, far from the modulation frequencies of 0.7 kHz and 1 kHz, which were chosen to modulate the FSS. This is an

important difference from other systems based on Doppler or FMCW radars that only detect passenger movement. Thanks to modulation, it is possible to distinguish the information of interest from the clutter, even when there are moving people or objects.

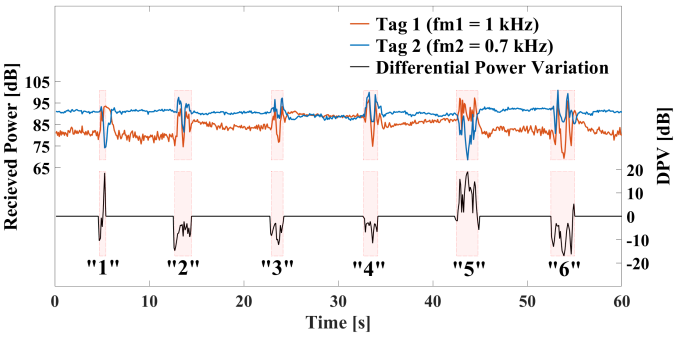

Fig. 12. DPV of Modulated FSS Tags for Driver Head Movement Detection

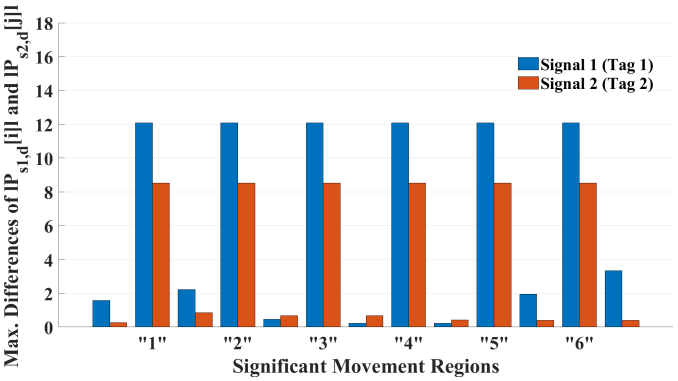

Fig. 13. Maximum Values of $P_{s1,d}[i]$ and $P_{s2,d}[j]$ Across Significant Movement Regions Highlighted in Figure 12.

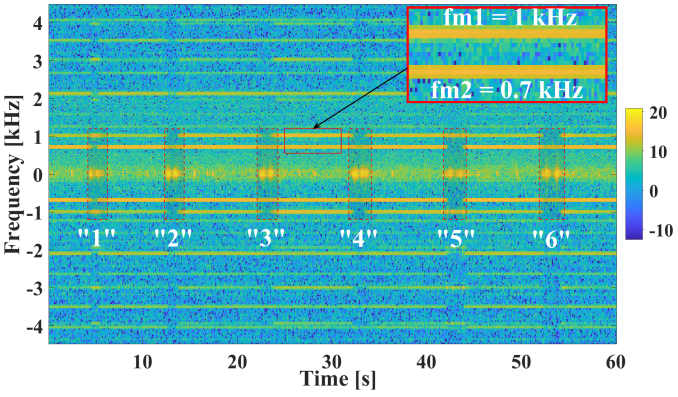

Fig. 14. Time-Frequency Spectrogram of DPV Signal for Driver Head Movement Detection

In the first scenario, shown in Fig. 15(a), the driver maintained focus on the road with controlled head movements. This included checking the right-side mirror, followed by a glance at the rearview mirror, and then another check of the right-side mirror. The DPV signal remained stable during forward gazes and showed clear variations corresponding to each head turn, with three significant movements recorded over two minutes.

TABLE V
OBSERVED DRIVER HEAD MOVEMENTS BY REGION AND THEIR BEHAVIORAL IMPLICATIONS

Region	Head Movement Detected	Observed Behavior and Implication
"1"	Leftward Mirror Check	Driver shifts head to the left to view the left-side mirror, indicative of situational awareness and lane-checking behavior.
"2"	Rightward Mirror Check	Head movement to the right towards the right-side mirror, reflecting attentiveness in monitoring adjacent traffic.
"3"	Rearview Mirror Check	Movement directed towards the center rearview mirror, demonstrating awareness of rear traffic flow and overall situational monitoring.
"4"	Center Console Display Check	Downward gaze to the dashboard or infotainment system, indicating a brief attention shift typical of standard in-vehicle interactions.
"5"	Leftward Roll Deviation	Controlled head tilt to the left, suggesting posture adjustment or enhanced mirror visibility, aligned with attentive driving behavior.
"6"	Rightward Roll Deviation	Controlled tilt to the right, supporting lateral awareness and posture adjustments associated with active monitoring of surrounding traffic.

Another movement related to the head is the one that can be detected when it suddenly falls. This type of movement is common in drivers with symptoms of severe drowsiness. Fig. 15(b) presents the results of tests simulating drowsiness through head movements such as rolling side to side and pitching down. Unlike lateral movements where the signal from one of the two FSS was blocked, in this type of vertical movement [?], there was an increase in the received power in both FSS as the direct line of sight was partially unblocked. Three regions can be observed during these drops: the first where the DPV difference was negative at the start of the movement, a second where there was more radar visibility presenting an almost null DPV difference, and positive DPV values when the head returns to the initial position.

An additional scenario, illustrated in Fig. 15(c), was conducted to assess the system's response during driver interactions with a passenger. In this case, the driver frequently turned his head toward the passenger and made subtle movements while speaking. These interactions resulted in noticeable lateral head movements and minor shifts, producing a DPV signal marked by increased variability and frequent, irregular fluctuations, capturing the distinctive movement patterns associated with conversational distractions.

The third scenario, shown in Fig. 15(d), evaluated the system's detection of mobile device interaction. Here, the driver repeatedly glanced downward to simulate phone use, leading to consistent dips in the DPV signal. These dips corresponded to downward pitch movements, and their repeated pattern highlights the system's effectiveness in identifying distractions from mobile device usage. This result suggests that the radar system can reliably detect head movements commonly associated with phone interaction, a frequent source of driver

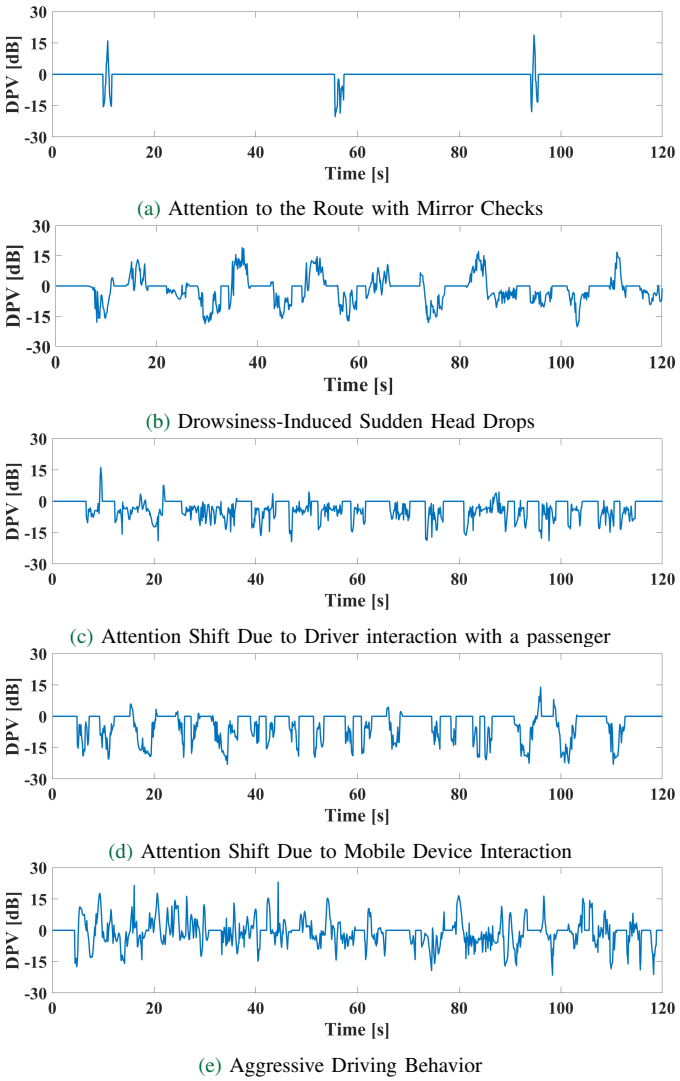

(a) Attention to the Route with Mirror Checks

(b) Drowsiness-Induced Sudden Head Drops

(c) Attention Shift Due to Driver interaction with a passenger

(d) Attention Shift Due to Mobile Device Interaction

(e) Aggressive Driving Behavior

Fig. 15. DPV Signal in Stationary Testing Phase Illustrating Driver Behavior Across Different Scenarios

distraction.

In comparison, the aggressive driving scenario illustrated in Fig. 15(e), produced a DPV signal with quick, sharp peaks, indicating sudden and intense head position changes. These signal variations were triggered by rapid head turns to the left and right, along with pronounced forward tilts, simulating behaviors like abrupt lane changes and sudden accelerations. The system effectively captured these intense, erratic movements, demonstrating its sensitivity to rapid yaw and tense pitch movements, which are characteristic of aggressive driving and deviate significantly from typical, controlled head movements.

Overall, the system demonstrates a robust capability to monitor and classify driver behavior through the analysis of significant head movements over time. The initial stationary testing phase validated the system's ability to accurately distinguish between attention and non-attention states in a controlled environment. This setup enabled safe testing of non-attention behaviors, such as mobile device interaction and conversational distractions, which would otherwise be challenging to assess in an active urban driving environment.

Building on these results, further experiments were conducted in a dynamic testing phase with the vehicle in motion on an urban main route. These on-road tests extended the evaluation to real-world conditions, allowing the system to demonstrate its effectiveness in detecting head movements associated with attentive driving behaviors under typical driving scenarios. The results in Fig. 16 present representative samples from the tests conducted on urban routes, highlighting the system's accuracy in identifying movement patterns characteristic of real-world driving. In Fig. 16(a) during a test on a straight road segment, the DPV signal remained relatively stable, with only occasional significant movements, indicating minimal and controlled head movements consistent with attentive driving on a straightforward path. In contrast, Fig. 16(b) illustrates a scenario involving a roundabout near the end of the route. Here, an increase in head movement activity, especially toward the test's conclusion, corresponds to the driver's need to check for traffic and navigate effectively. These examples from a broader set of tests highlight the system's responsiveness to different driving contexts and its adaptability to complex scenarios

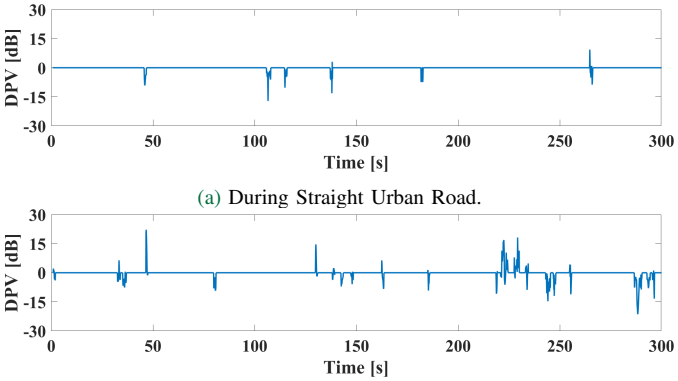

(a) During Straight Urban Road.

(a) During Urban Road with Turns and Maneuvering.

Fig. 16. DPV Signal in Dynamic Testing Phase in Urban Driving Conditions

To further illustrate the system's effectiveness in distinguishing between attention and distracted states, an indicator of sustained driver focus has been defined as the number of points detected over time in significant movement regions. This indicator represents the total number of points within significant movement regions over a specified observation period. These points are characterized by a DPV value that falls within the significant movement regions, meaning it is not equal to 0 dB.

The calculation for this indicator $I(T)$ is given by:

$$I(T) = \frac{1}{T} \sum_{i=1}^{M} \mathbf{1} \left(\text{DPV}(i) \neq 0 \, \text{dB} \right) \tag{12}$$

where:

- M is the total number of DPV points collected during the observation period T, set to a typical update interval to determine if an alarm needs to be triggered (2 minutes).
- $\text{DPV}(i)$ represents the DPV value at the i-th point.

Additionally, a statistical analysis of the I indicator distributions, based on extensive testing, showed that 50 lies near the upper quartile for attention states and the lower quartile for non-attention states, providing a robust quantitative basis for this threshold. Setting the threshold at 50 minimizes the likelihood of overlap between attention and non-attention states, thereby reducing misclassification errors and ensuring reliable distinction between driver attention levels.

Fig. 17 presents a box plot with the results, showing a comparison of this indicator across different driving scenarios, including both stationary and moving vehicle tests. This comparison highlights the system's ability to distinguish between attention-driving states and distracted or non-attention states based on the frequency and pattern of head movements. In attention states, a consistent number of points were detected within the significant movement regions, resulting in a steady count over time. In contrast, distracted states show irregular patterns, with fewer sustained movements captured within the significant movement regions.

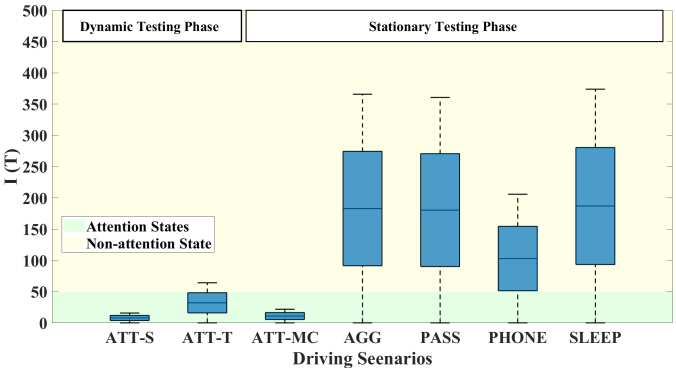

Fig. 17. Evaluating Driver Attention Levels Using a Significant Head Movement Indicator. Box plot with the following groups: ATT-MC: Driving on a Straight Urban Road, ATT-T: Driving on an Urban Road with Turns, ATT-MC: Attention to the Route with Mirror Checks, AGG: Aggressive Driving Behavior, PASS: Attention Shift Towards the Passenger, PHONE: Attention Shift Due to Mobile Device Interaction, SLEEP: Simulated through sudden head drops and drowsiness-related tilts Drowsiness.

The processing time required to compute I(T) at each observation period (120 seconds) is 114 ms using a laptop (Intel i7-1165G7 at 2.80 GHz). This introduces a minimal delay, comparable to the time needed to acquire a single sample. Therefore, the system can be implemented in microcontrollers for future commercial deployments. The distinct frequencies and patterns of movement across these scenarios underscore the system's capability to reliably differentiate between various attention levels, validating its robustness and adaptability for real-world applications. This differentiation in head movement patterns between attention and non-attention states suggests that the system can effectively serve as a driver monitoring tool, capable of providing timely alerts in response to changes in driver focus. Drowsiness occurs during long and monotonous periods of driving. In such cases, as the level of drowsiness increases, driving becomes more passive and involves fewer movements [?]. Therefore, the system could be useful to detect this low activity, and consequently the I(T) index would remain low.

Vehicle vibrations caused, for example, by acceleration, generate noise in the Doppler spectrum close to the carrier frequency, but interfere with the measurement of the signal at the modulation frequencies (0.7 kHz and 1 kHz). To investigate the effect of this interference, some experiments were conducted. An accelerometer (ST Microelectronics LSM303D) was mounted beside the radar to show the noise introduced by the car's vibrations. The radar targets the FSS mounted on the co-pilot's seat, which was empty. Both the driver's and rear seats were occupied by two passengers. Fig. 18 shows the variation of the acceleration, the signal from the two FSSs, and the detected DPV.

The measurement procedure was as follows: first, the vehicle was stopped with the engine off. The engine was then started, An increase in acceleration due to vibrations was observed, but the algorithm successfully avoided false alarms in the DPV signal. During the urban route, the system maintained accuracy, with the thresholds in Table IV ensuring no false detections, even while the vehicle was in motion. The only exceptions were minor false alarms caused by abrupt bumps, such as speed bumps at the entrances of roundabouts.

These strong peaks can be detected with the help of an accelerometer, and these time intervals could be ignored using the accelerometer information.

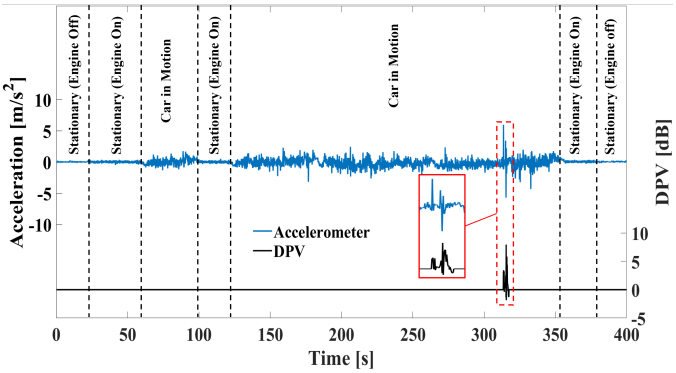

Fig. 18. Time-Series Analysis of Vehicle Vibration Signals: Accelerometer and DPV Response in Different Operating State

VI. Conclusion

This paper has introduced a novel driver monitoring system based on modulated FSS integrated with mmWave Doppler radar for real-time detection of driver head movements. The system leverages low-cost microcontrollers and distinct frequency modulation to accurately detect critical head gestures, enhancing the capabilities of ADAS for safer driving experiences. By focusing on only two modulation frequencies, the proposed approach significantly reduces computational complexity and improves clutter immunity, making it highly suitable for practical automotive applications. Experimental results demonstrate the system's ability to effectively monitor driver attention and detect potentially dangerous behaviors, such as distraction or aggression. The non-invasive and privacy-preserving nature of this solution ensures that it can be widely

adopted in modern vehicles without raising privacy concerns. The simplicity of the system, combined with its robustness, provides a cost-effective approach to improve road safety. Future work will aim to enhance the system's capabilities by enabling the recognition of a broader range of driver states, ensuring greater adaptability to diverse environments.

Farid Morabet received the Bachelor's degree in Physics and Electronic Science and the Master's degree in Telecommunication Systems Engineering from Abdelmalek Essaâdi University, Tetouan, Morocco, in 2018 and 2021, respectively. He is currently a Pre-doctoral Research Staff in Training with the Department of Electronic, Electrical, and Automatic Engineering at Rovira i Virgili University (URV), Tarragona, Spain, where he started in 2023. His current research interests include the development of advanced electromagnetic systems, millimeter-wave technologies, and innovative sensor applications.

From October 2022 to March 2023, he was awarded an Erasmus+ Mobility Grant for research collaboration at AntennaLab, Universitat Politècnica de Catalunya (UPC), Barcelona, Spain, focusing on wireless systems for biomedical applications.

Antonio Lazaro (M'07–SM'16) was born in Lleida, Spain, in 1971. He received the M.S. and Ph.D. degrees in telecommunication engineering from the Universitat Politècnica de Catalunya (UPC), Barcelona, Spain, in 1994 and 1998, respectively. He then joined the faculty of UPC, where he currently teaches a course on microwave circuits and antennas. Since July 2004, he is a Full-Time Professor at the Department of Electronic Engineering, Universitat Rovira i Virgili (URV), Tarragona, Spain. His research interests are microwave device modeling, on-wafer noise measurements, monolithic microwave integrated circuits (MMICs), low phase noise oscillators, MEMS, RFID, UWB and microwave systems.

Marc Lazaro was born in Tarragona, Spain, in 1995. He received the BS in Industrial Electronics and Automation Engineering and the MS in Electronic Systems Engineering and Technology (METSE) from Rovira i Virgili University, Tarragona, Spain, in 2017 and 2018, respectively. Up until now, he has accumulated professional experience as a data acquisition engineer and as embedded systems developer. Since 2019 he has been working toward the Ph.D. degree in the Department of Electronics at the Rovira i Virgili University. His research activities are focused on semipassive RFID technologies based on backscattering communication and novel applications based on mmWave identification (MMID).

Ramon Villarino was awarded a degree in Telecommunications Technical Engineering by Ramon Llull University (URL) in Barcelona, Spain, in 1994, a degree in Senior Telecommunications Engineering by the Universitat Politècnica de Catalunya (UPC) in Barcelona, Spain, in 2000 and a doctorate by the UPC in 2004. In 2005-2006, he was a Research Associate at the Technological Telecommunications Center of Catalonia (CTTC) in Barcelona, Spain. He worked as a Researcher and Assistant Professor at the Universitat Autònoma de Barcelona (UAB) from 2006 to 2008. Since January 2009 he has been a full-time professor at Universitat Rovira i Virgili (URV) in Tarragona, Spain. His research activities focus on radiometry, microwave devices, and systems based on UWB, RFIDs, and frequency selective structures using MetaMaterials (MM).

David Girbau (M'04–SM'13) was awarded a BSc in Telecommunication Engineering, a Master's in Electronics Engineering, and a doctorate in Telecommunication by Universitat Politècnica de Catalunya (UPC) in Barcelona, Spain, in 1998, 2002 and 2006, respectively. From February 2001 to September 2007 he was a Research Assistant at UPC. From September 2005 to September 2007 he was a part-time Assistant Professor at Universitat Autònoma de Barcelona (UAB). Since October 2007 he has been a full-time professor at Universitat Rovira i Virgili (URV) in Tarragona, Spain. His research interests include microwave devices and systems, with an emphasis on UWB, RFIDs, RF-MEMS and wireless sensors.